sustainability

MDPI

Article

Effects of Olivine Alteration on Micro-Internal Structure and Geomechanical Properties of Basalts and Strength Prediction in These Rocks

Kadir Karaman [1,*] and Hasan Kolaylı [2]

[1] Department of Mining Enginnering, Karadeniz Technical University, Trabzon 61080, Turkey
[2] Department of Geology Enginnering, Karadeniz Technical University, Trabzon 61080, Turkey; hkolayli@ktu.edu.tr
* Correspondence: kadirkaraman@ktu.edu.tr; Tel.: +90-462-377-4264

Abstract: Understanding the variations of the geomechanical properties of rocks in geotechnical projects from the perspective of their micro-structures and alteration conditions is crucial for ensuring the safety and long-term sustainability of rock engineering (e.g., tunnels, slopes, mining). This study was carried out on basaltic rocks from the Akcakale and Mersin vicinities in Trabzon City to investigate the geomechanical and mineralogical properties in comparison with the uniaxial compressive strength (UCS). This study was conducted in three different locations (A1, M2, and M3) where the basaltic rocks outcrop belongs to the same lithological formation. During this study, quite different results were obtained from the basalt samples taken from different sites and the reasons for these differences were examined by petrographic, SEM (Scanning Electron Microscopy), and EDS (Energy Dispersive Spectroscopy) analyses. Since the number of comprehensive studies on basalts is very limited, this study aims to investigate practical and useful equations in the estimation of the UCS for various alteration conditions. Statistically, significant relationships were observed between geomechanical properties with the UCS and serpentinization rate (SR). This study revealed that the serpentinization of the olivine mineral is the most important factor causing the differences in the experimental results. The proposed equations for estimating the UCS are particularly significant for geotechnical applications where direct sampling is challenging, such as in weak-rock environments.

Keywords: sustainability of rock engineering; basalt; uniaxial compressive strength (UCS); serpentinization of olivine; geomechanical properties

Citation: Karaman, K.; Kolaylı, H. Effects of Olivine Alteration on Micro-Internal Structure and Geomechanical Properties of Basalts and Strength Prediction in These Rocks. *Sustainability* **2024**, *16*, 5490. https://doi.org/10.3390/su16135490

Academic Editors: Martina Inmaculada Álvarez Fernández and Víctor Martínez-Ibáñez

Received: 12 May 2024
Revised: 2 June 2024
Accepted: 14 June 2024
Published: 27 June 2024

Copyright: © 2024 by the author. Licensee MDPI, Basel, Switzerland. This article is an open access article distributed under the terms and conditions of the Creative Commons Attribution (CC BY) license (https://creativecommons.org/licenses/by/4.0/).

1. Introduction

The sustainability of rock engineering is an emerging trend in future development, as proper designs in geotechnical engineering not only lead to improvements in stability and safety, but also reduce costs, extend the life of mines, and protect the environment [1,2]. Sustainability in geotechnical engineering emphasizes the long-term performance and durability of structures such as tunnels, rock slopes, bridges, and benches at mine pits or quarry sites. The geomechanical properties of rocks are widely used by rock engineers in the design of geotechnical studies. The uniaxial compressive strength (UCS), point load strength index (PLI), Schmidt hammer rebound number (R), direct or indirect tensile strength (BTS), density, apparent porosity, and ultrasonic pulse velocity (UPV) of rocks are some of the momentous geomechanical parameters used in the design. However, the UCS of the rock material is one of the most critical parameters among the other geomechanical properties, and it is highly regarded for various issues encountered during excavation, blasting, and support systems in rock engineering applications [3–5]. The UCS can be found experimentally through direct or indirect tests [6]. Nevertheless, the direct de-

termination of this parameter in the preliminary design of a geotechnical project is relatively expensive, troublesome, and time-consuming. Moreover, being recommended NX-sized (54.7 mm) core samples from the problematic ground (weak, highly fractured, and thinly bedded rocks) is widely challenging as the test necessitates high-quality core samples. Therefore, indirect test methods such as PLI, BTS, and R are often used to predict the UCS due to their more straightforward, faster, and more economical solution aspects [7–9].

The geomechanical properties of rocks change as they are heterogeneous materials by nature due to their mineralogical composition, alteration, porosity, texture, grain size, shape, and degree of grain interlocking, etc., [10–12]. It was mentioned that rock characteristics such as porosity, the amount of saturation, texture, mineralogical composition, temperature, and degradation have an impact on the rock strength [13]. Several studies [10,14] researched the relationship between the rock strength and mineral grain size. Brace [15] showed that fine-grained rocks have a higher strength in comparison with coarse-grained ones. The relationships between the mechanical properties and mineralogical composition of various rock types were explored and different models were established to estimate the UCS depending on the mineral composition [16]. Tugrul and Zarif [10] reported that the mineralogical content is one of the significant petrographical characteristics of rocks with an impact on the rock strength. However, Ulusay et al. [17] stated that the effect of the textural properties of rocks appears to be more crucial than the mineralogy for evaluating the geomechanical properties.

Basalt is one of the most common rocks found in the earth's crust and has been utilized for various engineering applications in the highway basement and railroad ballast, cement aggregate production, pavement construction, and rock fill for dams [18]. Numerous studies have been carried out on basalts for different purposes. Matin and Manga [19] observed that the strength of vesicles in basaltic flows is considerably affected by their porosity. Gurocak and Kilic [20] investigated the effect of weathering on the geomechanical properties of the Miocene basalts and found good linear relationships between the weathering degree of the basalts and their geomechanical properties. Juneja and Endait [21] examined the connection between the UPV and the physical properties of vesicular basalt. The results demonstrated an increase in the UPV with an expanding dry density and the contrary pattern with expanding apparent porosity. Murthy et al. [22] studied the effect of porosity on the engineering properties of vesicular and amygdaloidal basalts and observed that a good level of correlation is obtained for the UCS, elastic modulus, and Poisson's ratio in basalts with porosity >8–10%, except for the UPV. Pathiranagei et al. [23] investigated the effect of different temperatures on the engineering properties of basalt. They reported that the threshold temperature at which the engineering properties of rocks begin to deteriorate is 500 °C for basalt. Tahir and Karaman [24] examined the variation of the UCS/PLI ratio (k) for basalts from a regional and global perspective and indicated that the optimal k ratio should be in the range of $17 \leq k \leq 20$ for the basalts according to the ANOVA results. Liu et al. [25] investigated the effects of amygdale heterogeneity and the sample size on the mechanical properties of basalt. Tarawneh et al. [26] focused on the main engineering characteristics of basalt rocks to shed some light on their properties and reported that basalt has good physical and mechanical properties that can be used for engineering applications. Ye et al. [27] evaluated the differences in the permeability and mechanical strength characteristics of basalt before and after CO_2 mineralization. Sharo and Al-Tahawa [28] mentioned that although many relationships have been established between the UCS and other geomechanical properties of numerous types of rocks, there is still a need to develop equations between the UCS and other parameters in basaltic rocks.

Basaltic rocks used in a variety of engineering applications are common in the east of Turkey, especially in the Eastern Black Sea Region. When the studies on basalts in the literature are examined, it is clear that detailed studies are needed on the relationships

between the UCS and geomechanical properties of basalts, especially for progressive alteration conditions. Considering the previous studies, it is understood that the rock parameters (UCS, weathering/alteration, porosity, and p-wave velocity) that affect each other have generally been studied. Therefore, in this study, in addition to the geological observations made in the field, the causes of the formation of features affecting the geomechanical properties of basalts such as porosity were investigated in detail by SEM (Scanning Electron Microscopy), EDS (Energy Dispersive Spectroscopy), and petrographic thin-section analyses. Therefore, the effects of olivine alteration (serpentinization), which are variables found in basalts, on the geomechanical properties, mineral structure, and chemical content were investigated. In addition, the structural and geological reasons for the different properties obtained from basalts taken from different points of the same geological formation as well as the importance of sampling were emphasized.

2. Experimental Studies

2.1. General Geology and Sampling Location

In the current study, basalt samples of aged Eocene were selected from three different zones within the boundaries of Akçakale and Mersin Neighborhood within the geological units. Basalts were found in the form of prismatic dykes in Eocene basalt and pyroclastic forms. The thickness of the dykes varied between 12 and 15 m, and the spread area of each is more than 1 hectare. As seen in Figure 1, basalt blocks were taken from three different locations in Trabzon (Eastern Black Sea Region of Turkey) (Akçakale 1 (A1), Mersin 2 (M2), and Mersin 3 (M3)). Basalt blocks were checked for macroscopic flaws such as weathering, fractures, and cracks.

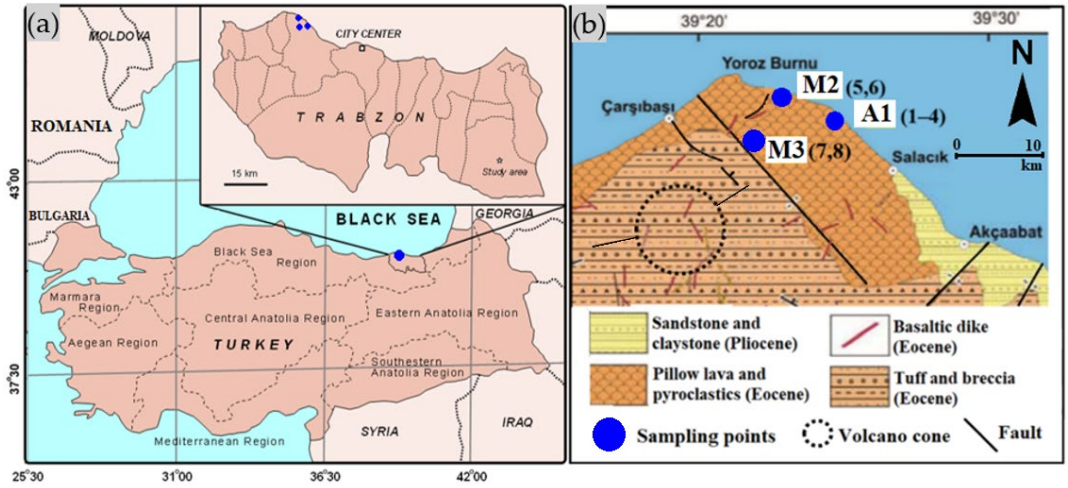

Figure 1. Study area location map (**a**) and geological properties of the study area (modified from Yücel et al. [29] (**b**).

A laboratory core drilling machine was utilized for obtaining core samples with NX dimension (54.7 mm). Samples' ends were ground flat and made parallel to each other before tests. Moreover, a comparator was used to check the cut-end faces of the core samples in terms of smoothness. To obtain optimal findings and enable accurate comparisons, the tests were performed under dry and saturated circumstances.

2.2. Geomechanical Tests of Basalts

Laboratory experiments involved the tests for uniaxial compressive strength (UCS), point load index (PLI), Brazilian tensile strength (BTS), density (ϱ), apparent porosity (n), Schmidt rebound hardness (R), Leeb hardness (HL), and P wave velocity (UPV) of the rock samples under both dry and saturated test conditions (Table 1, Figure 2). According to Table 1, basalt samples numbered 1 to 4 belong to A1, 5 and 6 to M2, and 7 and 8 to M3.

Core samples with length-to-diameter ratios of 2.5 were used in the determination of UCS values [6]. A computerized servo control machine with a 300-ton load capacity was utilized at a stress rate of 0.75 MPa/s. The average UCS value was computed by averaging the 5 tests on the same rock block.



Figure 2. A view of laboratory studies: some basalt core samples in the oven (**a**), after UCS test (**b**), BTS test (**c**), SEM analysis (**d**), Leeb hardness (**e**), and UPV test (**f**).

Table 1. Results of experimental studies.

Rock Code	UCS (MPa) Dry-Sat.	PLI (MPa) Dry-Sat.	BTS (MPa) Dry-Sat.	UPV (m/s) Dry-Sat.	R Dry-Sat.	H_L Dry-Sat.	ϱ (g/cm³) Dry-Sat.	n (%)
1	167–145	8.9–7.8	14.2–12.4	5904–6131	44–42	835–789	2.90–2.91	0.65
2	184–130	10.3–9.5	14.8–14.5	5932–6088	43–41	812–770	2.89–2.90	0.66
3	185–132	9.9–9.6	12.1–11.0	5905–6116	42–39	826–802	2.88–2.89	0.84
4	180–150	9.5–8.7	11.8–11.2	5665–6118	45–42	848–807	2.91–2.92	0.75
5	139–69	4.5–3.7	8.9–7.7	4945–5653	40–38	720–663	2.80–2.82	2.48
6	100–56	3.8–3.3	8.3–7.5	4567–5394	37–34	700–641	2.79–2.81	3.11
7	60–33	2.9–1.6	8.1–5.5	3856–4671	24–20	620–580	2.78–2.82	4.22
8	51–25	2.7–1.3	7.4–3.1	3365–4430	19–15	570–501	2.78–2.81	5.29

Prior to the UCS test, UPV tests were applied to the core samples using the PUNDIT plus device. The core samples' ends were polished to provide a smooth surface before the measurements. To provide full contact and to remove the air gap between the sample surface and the transducers, a thin layer of Vaseline jelly was applied to the transducers' surface (receiver and transmitter).

The axial method of PLI testing was performed using a digital test apparatus according to the ISRM [6]. After the uncorrected PLI values were obtained, they were corrected to the equivalent diameter (De, 50 mm). The following equations were used in the determination of basalts' PLI (I_S) values.

$$I_s = \frac{P}{De^2} \quad (1)$$

$$F = (D_e/A)^{0.45} \quad (2)$$

$$I_{s(50)} = F \times I_s \quad (3)$$

where P is the applied load at failure in kN, F is the correction factor, and De is the equivalent core diameter in mm^2 ($De^2 = 4A/$).

To determine the indirect tensile strength, the BTS test was applied on a circular core sample which was put between two platens with loaded compression, generating a nearly uniform distribution of tensile stress. The mean BTS value was obtained by averaging ten core samples with a diameter-to-height ratio of 2 at a stress rate of 200 N/s.

$$\sigma_t = \frac{2P}{\pi Dt} \quad (4)$$

where P is the failure load, and t and D are the thickness and diameter of the core.

Leeb hardness (H_L) is a surface hardness meter that is specified by a non-destructive testing tool regarded as the Leeb Hardness Tester. The following equation was used in the determination of the corresponding H_L value of the samples [30]:

$$H_L = (Vr/Vi) \times 100 \quad (5)$$

A cylindrical tungsten impact body is launched to the surface by spring force and calculates the rebound and impact velocities (Vr and Vi, respectively). Twenty single-impact readings were obtained from the test surface and the mean value was recorded as the HL value of the samples [31]. The Schmidt hammer was periodically checked using the test anvil. All tests were performed with the hammer held vertically downward using the L-type hammer in the laboratory on NX-size (54.7 mm diameter) core samples. According to the ISRM [6], it is recommended to record 20 rebound values from single impacts separated by at least a plunger diameter and average the upper ten values. Core samples (a total of 40 samples) used for UCS and UPV tests were also utilized in the determination of apparent porosity (n %) and dry and saturated density with Caliper and saturation techniques. The apparent porosity is described as a percentage of the relation of the volume of the open pores in the sample to its exterior volume.

$$\text{Porosity, \%} = (W_S - W_D)/V \times 100 \quad (6)$$

where W_S is the saturated weight, W_D is the dry weight, and V is the volume of the test of the samples. Volume of open pores, $cm^3 = (W_S - W_D)$.

2.3. Petrographic Examination of Basalts

The naming of the rocks, mineral types, alteration constituents, and texture properties (grain size distribution, perimeter of mineral phases, and micro-cracks), which would lead to the effect of engineering properties of rocks, were examined by petrographic thin-section studies (Figure 3). According to the petrographical investigations, all the samples examined have olivine augite basalt character and have micro-granule–microlithic porphyric texture. They consist primarily of labradorite, olivine, augite, biotite, and opaque (magnetite) minerals (Table 2). Thin-section analyses showed that the essential minerals present are labradorite (plagioclase) (46–50%), augite (25–28%), olivine (18–20%), and biotite (2–3%) in Akçakale basalts (A1). The rate of serpentinization in olivines is in the range of 5–10%. M2 basalts are composed primarily of augite 26–27%, olivine 19–20%, and biotite 3%. The serpentinization rates of olivines are in the range of 15–35%. The mineralogical contents of M3 basalts are augite (28%), olivine (20%), and biotite (3%). Olivine has

altered to serpentinization in the range of 70–80% in M3 basalts. Opaque mineral composition in all sections generally varies between 2% and 3%. The total area percentage of vesicles for all samples is in the range of 1–2%. Furthermore, the serpentinization rate of the olivines present in the micro-granule–microlithic paste of the basalts in all three regions is approximately equal to the serpentinization rate in the total rock.

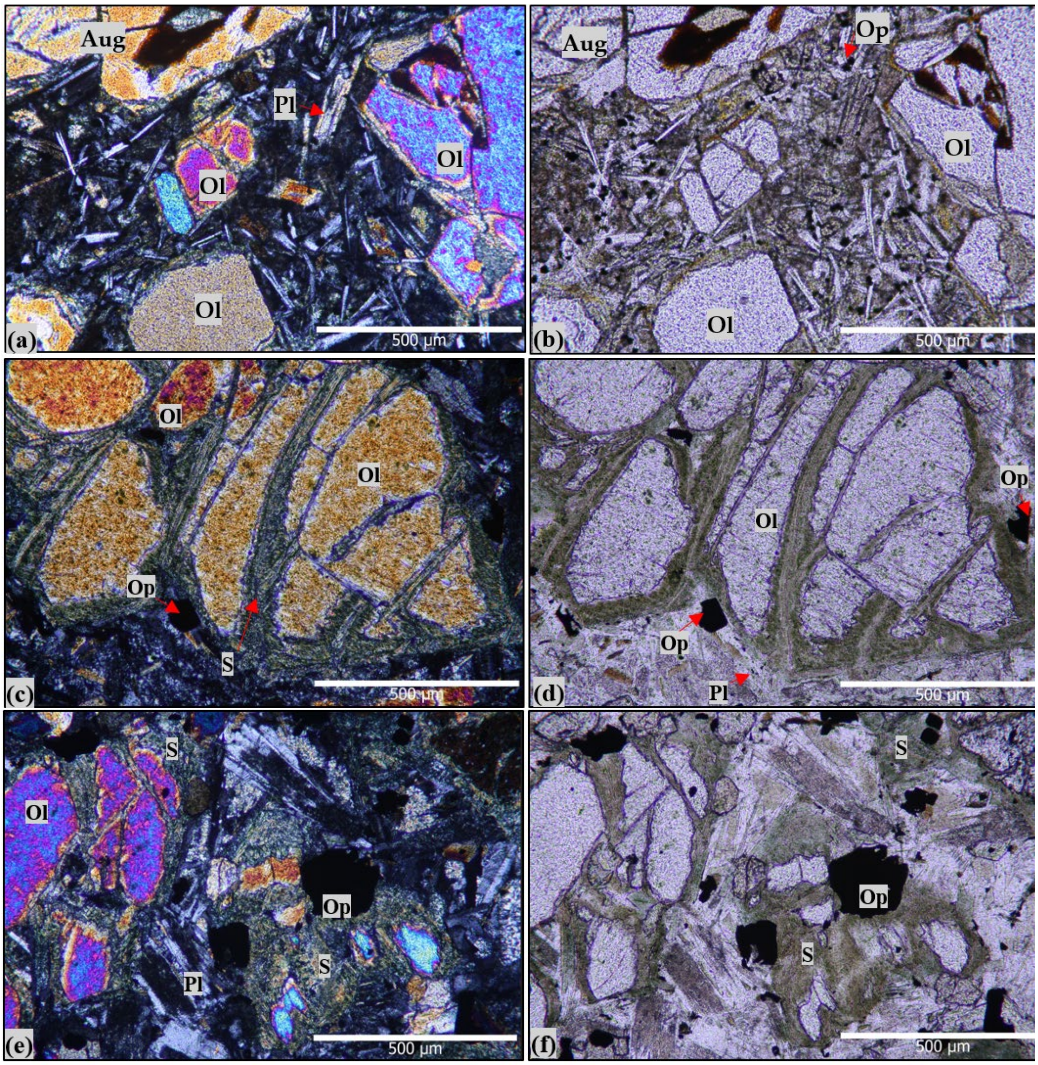

Figure 3. Microscopic images of basalts with serpentinization rates (SR) of olivine; A1 basalts (cross-polarized light (**a**) and plane-polarized light (**b**)), M2 basalts (**c**,**d**), M3 basalts (**e**,**f**), Pl: plagioclase, Ol: olivine, Aug: augite, Op: opaque mineral, and S: serpentine.

Table 2. Thin-section analysis results of basalts.

Minerals	Mineral Contents of Selected Samples (%)							
	Akçakale 1 (A1)				Mersin 2 (M2)		Mersin 3 (M3)	
	1	**2**	**3**	**4**	**5**	**6**	**7**	**8**
Labradorite	49	50	48	47	46	48	46	47
Augite	25	27	25	28	26	25	28	27
Olivine	20	18	20	18	20	19	20	19
Opaque	3	2	2	3	3	3	2	2
Biotite	2	2	3	2	3	3	2	3
Vesicle	1	1	2	2	2	2	2	2
SR	5	5–10	10	10	15–20	25–35	70–75	70–80

SR: serpentinization rate of olivine.

2.4. Statistical Analysis of Basalts

Predictive analytics software (PASW Statistics 23) was used to confirm statistically derived equations. All variables of the rocks were found to be normally distributed according to the Kolmogorov–Smirnov Z test and were then subjected to parametric statistical tests. Linear, power, and exponential relationships were examined between the variables to obtain the most reliable equations. ANOVA tables were checked to see whether regression models are significant or not. Similarly, the significance of coefficients in equations was examined as well.

3. Results and Discussion

3.1. General Evaluation of the Test Results

In this study, eight basalt rock blocks taken from Akcakale (A1) and Mersin (M2 and M3) vicinities were analyzed. It is seen in Table 2 that the first four basalt samples have similar engineering properties as a result of the textural and mineralogical characteristics, as well as low porosity values (n < 1%). However, the geomechanical properties of basalt samples can be affected by a variety of textural and mineralogical characteristics [31]. According to the mineralogical examinations, Mersin basalts (M2 and M3) show a large scale of alteration (serpentinization) in olivine minerals as well as porosity values ranging from 2.48% to 5.29%. Therefore, the engineering properties values of Mersin basalts, except for porosity, are lower than those of Akcakale basalts (A1 basalts). The A1 basalts, having n < 1%, exhibited high variations in their engineering properties.

When all results from different types of basalts are considered, the mean UCS values vary between 51 and 185 MPa for dry and between 25 and 150 MPa for saturated conditions. According to ISRM [6], basalts are understood to belong to high- or very-high-strength classes, except M3. The mean PLI values range between 2.7 and 10.3 MPa when dry rock samples are considered, while this value is between 1.3 and 9.6 MPa for saturated rock samples. BTS values are changed from 7.4 to 14.8 MPa and from 3.1 to 14.5 for dry and saturated basalt samples, respectively. The density values of the basalts are between 2.78 and 2.91 for dry samples, and 2.81 and 2.92 for saturated samples. The average n rate of basalts ranges from 0.65% to 5.29%. Korkanc and Tugrul [32] indicated that basalts commonly have higher densities than others. As in the study of Toft et al. [33], at high degrees of serpentinization, lower density values are obtained in this study. The R-value varies between 19 and 45 and 15 and 42 for dry and saturated basalts, respectively. The HL values range between 570 and 848 and 501 and 807 for dry and saturated basalts, respectively. The UPV values for dry samples vary between 3365 and 5932 m/s, while this value is between 4430 and 6131 m/s for saturated basalts.

3.2. Assessment of the Relationships between Data Pairs

The relationships between the UCS and geomechanical parameters (PLI, BTS, ϱ, n, R, HL, and UPV) were investigated both for dry and saturated conditions (Figures 4 and 5).

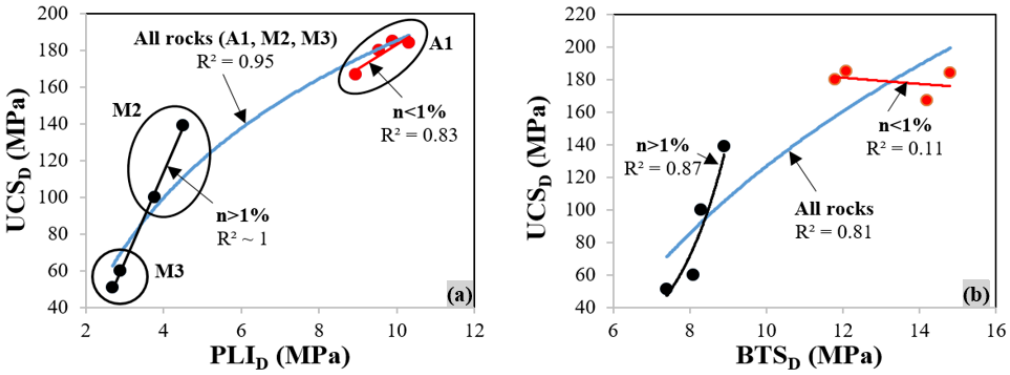

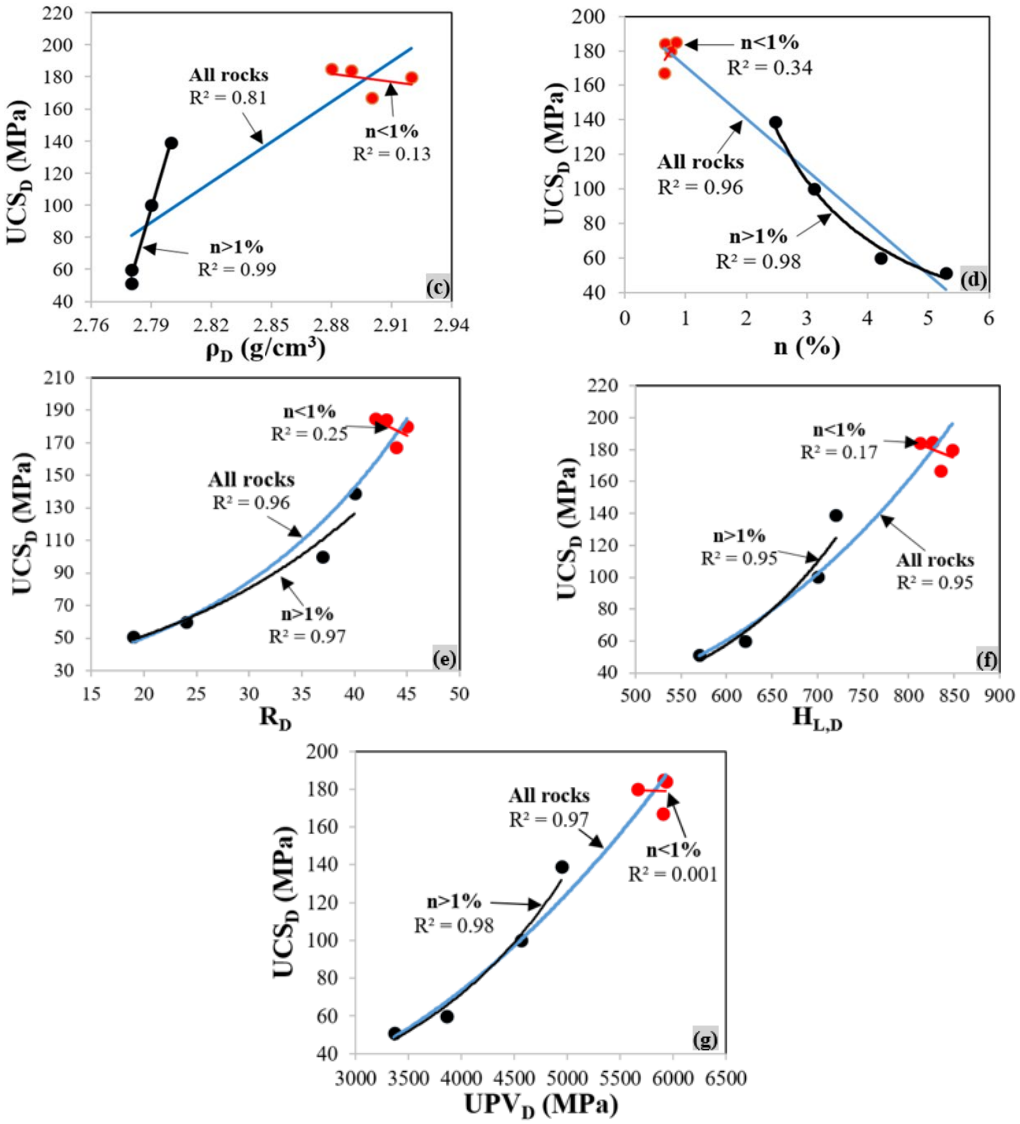

Figure 4. Relationships between UCS$_D$ and geomechanical properties (**a**–**g**).

The coefficient of determination between the UCS and the basalts' geomechanical parameters varied between 0.81 and 0.97 for the dry samples (Figure 4). Similarly, this value ranged from 0.91 to 0.99 for the saturated samples (Figure 5). As expected, a negative relationship was obtained between the UCS and n, while positive statistical relationships were obtained between the UCS and other geomechanical properties. Regression analyses were performed for each data pair for three different cases (for all basalts with equations, for basalts with a porosity below 1%, and basalts with a porosity above 1%), although only the analyses for all basalts were considered in the statistical analyses.

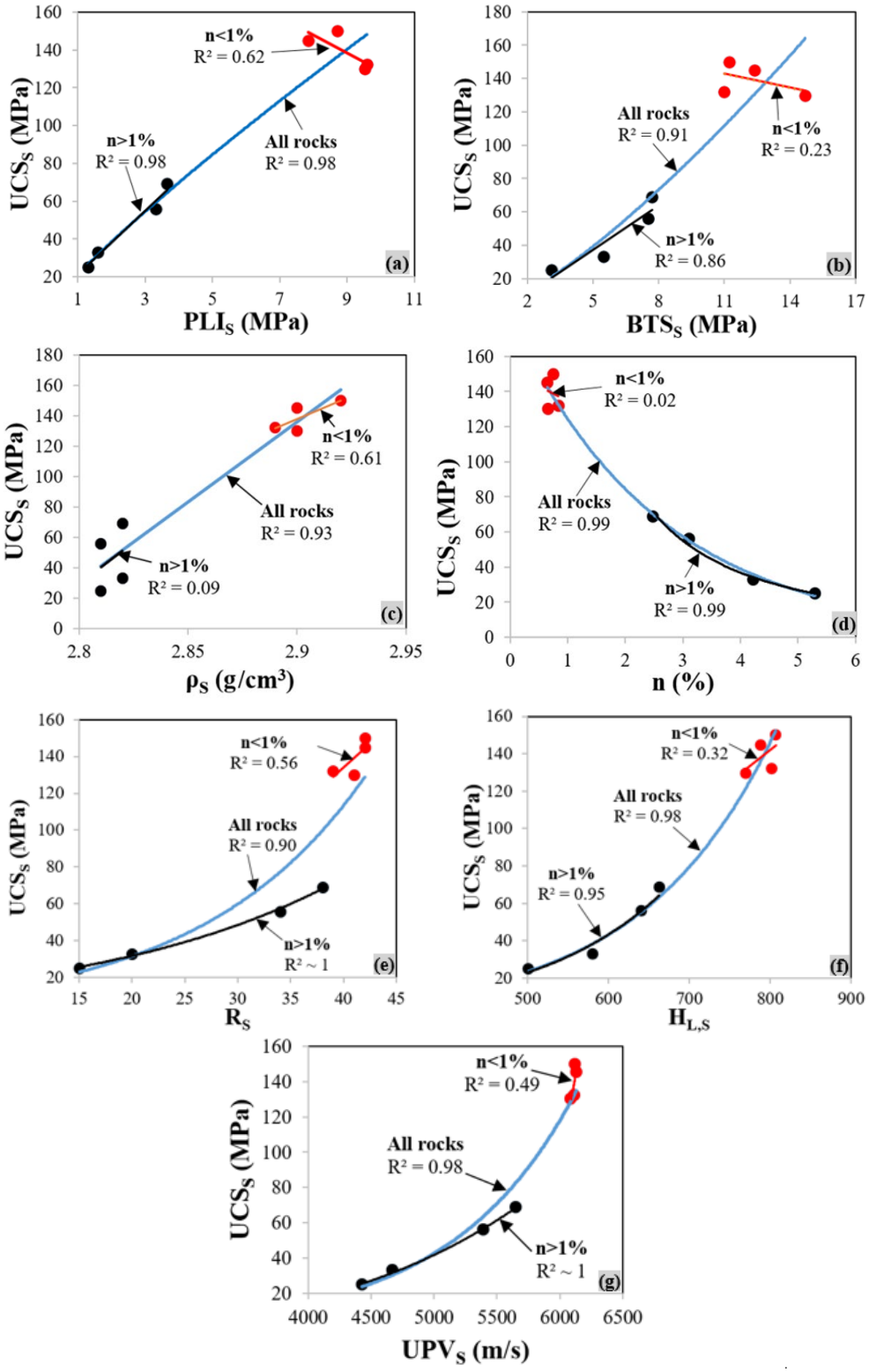

Figure 5. Relationships between UCSs and geomechanical properties (**a**–**g**).

In this study, high to very high regression relationships were obtained in all basalts, while generally, no significant relationships were obtained in A1 basalts with a porosity below 1%. However, in basalts with a porosity above 1% (2.48–5.29%), very high regression relations were generally obtained. In Figures 4a–c and 5e, two separate trends were found, one for all basalts and another for basalts having an n higher than 1%. Kahraman et al. [34] correlated the UCS with PLI for the rocks for both n >1% and n < 1%. They found

fairly good relationships between the data pairs for n >1% (R^2 = 0.75) and n < 1% (R^2 = 0.72). Similarly, only PLI values gave a high relation coefficient (R^2=0.83) for basalts with n<1%. Kılıc and Teymen [35] reported that even though a high coefficient is attained from the relations, it may not be proper for rocks with n < 2%. Karaman and Kesimal [11] also reported that there is a good relationship among the geomechanical properties of different rocks for n > 1%; however, no relationship was observed for the rocks with n < 1% values.

In the petrographic thin-section analyses, olivine serpentinization (SR) was observed at varying rates in basalts from three different sites (A1, M2, and M3), and the SR effect on the geomechanical properties was investigated. Strong relationships (R^2 = 0.91–0.97) were found between the progressive serpentinization of olivine minerals and geomechanical properties for all samples with an average of A1, M2, and M3 (Figure 6). However, only some important parameters (UCS, n, and UPV) are included in the graphs because other graphs are similar. Diamantis et al. [36] performed correlation analyses between the cohesion and internal friction angle in ultramafic rocks with serpentinization rates ranging from 3% to 92% and obtained high correlation coefficients (R^2 = 0.86–0.93).

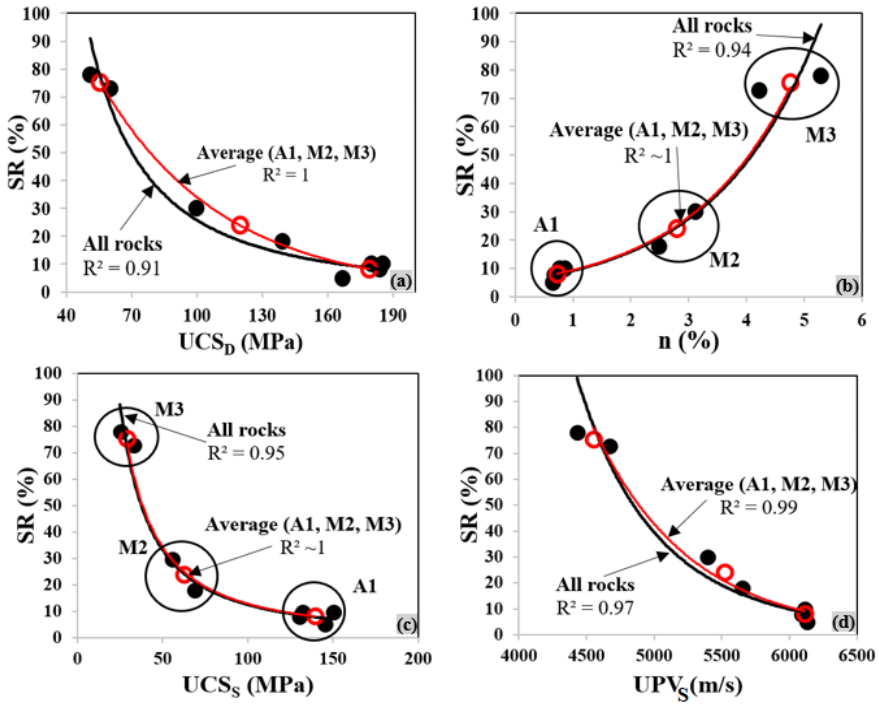

Figure 6. Relationships between olivine serpentinization and some geomechanical properties (**a**–**d**).

The petrographic thin-section analysis showed that the average serpentinization of olivine is 75.5 percent in M3 basalts, although this content is 8 percent in A1 basalts. This study revealed that the UCS dry samples of A1 basalts is about three times greater than those of M3 basalts with the high serpentinization of olivine and micro-cracks, while the difference increases even more in saturated samples. Statistically significant relationships (SL < 0.05) between the UCS and geomechanical parameters and the SR and geomechanical parameters were determined with 95% safety according to the statistical analyses (Table 3). When the statistical analyses for dry and saturated samples were evaluated separately, the average coefficients of determination were found to be 0.92 for dry samples and 0.95 for saturated samples, and the F values were found to be 115 and 274 for dry and saturated samples, respectively. According to the numerical values, the relationship of the parameters determined from the basalt samples in the saturated state with the rock strength is higher than in the dry state. Based on Table 3, the nonlinear equations have a higher prediction capability in the UCS estimation than those of the linear equations. Since

a higher relationship is expected for rocks with n >1%, the statistical analyses were also performed for these rocks in this study. Although the coefficient of determination was higher in basalts with n>1%, where the number of data was lower, as expected, the SL values obtained from all rocks were statistically more reliable at a 95% confidence interval.

Table 3. Results of statistical analyses.

Data Pairs	Equations	R.Type	R^2	ANOVA All Values		ANOVA n > 1%
				F	SL	SL
UCS_D–PLI_D	$UCS_D = 93.5In(PLI_D)-30$	Logarithmic	0.95	109.489	0.000	0.000
UCS_D–BTS_D	$UCS_D = 185ln(BTS_D)-300$	Logarithmic	0.81	24.810	0.003	0.068
UCS_D–ϱ_D	$UCS_D = 834\ \varrho_D - 2237$	Linear	0.81	25.014	0.002	0.005
UCS_D–n	$UCS_D = -30.1\ n + 201$	Linear	0.96	157.779	0.000	0.009
UCS_D–R_D	$UCS_D = 17.762e^{0.052R_D}$	Power	0.96	132.445	0.000	0.016
UCS_D–$H_{L,D}$	$UCS_D = 2 \times 10^{-8}\ H_{L,D}^{3.4125}$	Power	0.95	126.151	0.000	0.026
UCS_D–UPV_D	$UCS_D = 2 \times 10^{-7}\ UPV_D^{2.3729}$	Power	0.97	226.823	0.000	0.012
UCS_S–PLI_S	$UCS_S = 21.153\ PLI_S^{0.8609}$	Power	0.98	280.629	0.000	0.008
UCS_S–BTS_S	$UCS_S = 4.6503\ BTS_S^{1.3255}$	Power	0.91	59.201	0.000	0.035
UCS_S–ϱ_S	$UCS_S = 1055\ \varrho_S - 2922$	Linear	0.93	79.111	0.000	0.702
UCS_S–n	$UCS_S = 183.05e^{-0.387\ n}$	Exponential	0.99	791.034	0.000	0.006
UCS_S–R_S	$UCS_S = 8.7832e^{0.0639\ R_S}$	Exponential	0.90	56.246	0.000	0.002
UCS_S–$H_{L,S}$	$UCS_S = 1.1217e^{0.0061H_{L,S}}$	Exponential	0.99	389.417	0.000	0.024
UCS_S–UPV_S	$UCS_S = 0.3e^{0.001UPVS}$	Exponential	0.98	263.197	0.000	0.003
SR—UCS_D	$SR = 144{,}051\ UCS_D^{-1.9}$	Exponential	0.91	179.514	0.000	0.006
SR—UCSs	$SR = 8261.5\ UCSs^{-1.409}$	Power	0.95	106.085	0.000	0.008
SR—UPVs	$SR = -0.043\ UPVs + 266$	Linear	0.97	214.794	0.000	0.006

R. Type: Relation type, SL: Significance level.

To check the predictive ability of the developed formulas, scatter plots of measured and predicted UCS values were analyzed. Data points should ideally be distributed around a 1:1 diagonal straight line on a graph of measured and predicted values. A systematic deviation from the 1:1 line indicates that larger errors tend to accompany larger forecasts, indicating non-linearity in one or more variables. Two example graphs for dry and saturated conditions for UCS values measured in the laboratory and predicted using the equations are given in Figure 7. As illustrated in Figure 7a,b, the data points are almost evenly distributed around the 1:1 line, indicating that the Equations are valid. Therefore, it appears that statistically significant equations can be reliably used to predict the strength of basalts with variable serpentinization in olivines.

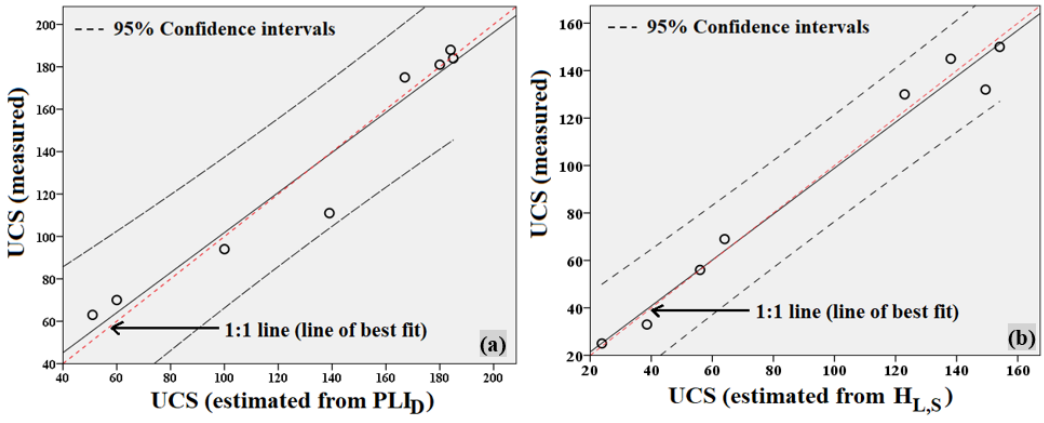

Figure 7. Measured and estimated UCS from PLID (**a**) and HL, S (**b**).

3.3. Effect of Olivine Serpentinization on the Geomechanical Properties of Basalts

It is widely known that olivine is a highly sensitive rock mineral for alteration. Serpentine, one of the main alteration forms of olivine, is formed along the fracture as a result of hydrothermal processes and can completely transform olivine-containing rocks into serpentine rocks [37]. Serpentine alterations can be described by the reaction:

$$2Mg_2SiO_4\ (\text{Olivine}) + 3H_2O = Mg_3Si_2O_5(OH)_2\ (\text{serpentine}) + Mg(OH)_2 \quad (7)$$

During serpentinization, large amounts of water are absorbed into the rock, the volume increases, the density decreases, and the original structure is destroyed [38]. Serpentinization is most effective in fractured rocks that allow water to percolate rapidly [38,39]. In near-surface environments, serpentinization can occur at temperatures from ~20 °C to greater than 400 °C [40]. When geologic systems are obducted onto the continents as ophiolites, low-temperature serpentinization occurs near the surface due to chemical weathering by meteoric water [41]. Serpentine has a lower density than olivine. Serpentinization in a closed system is, therefore, expected to increase in solid volume by about 50% [42]. This volume change has some consequences for fluid pathway evolution during serpentinization. It leads to an increase in porosity filling by reaction products and stress accumulation leading to cracking [43,44]. Tarawneh et al. [26] reported that the high values of porosity and void ratio values are related to the type of basaltic materials and degree of weathering. Since serpentinization will cause the internal expansion of rocks, microcracks are thought to have developed due to the pressure formed within the rock. The studies show that porosity is one of the key characteristics that affect rock parameters [11,45]. It is mainly controlled by the presence of both vesicles and micro-cracks [46]. Porosity also controls the mechanical response of materials, so that as porosity increases, their strength decreases and their elasticity increases [47]. In this study, serpentinization, which is the most important cause of porosity, was revealed by the analysis. Similarly, Hatakeyama and Katayama [48] studied pore fluid effects on the oceanic lithosphere and reported that serpentinization could lead to the development of pore spaces during hydration reactions, which influences the UPV. Tendhorey et al. [49] reported that the intensity of the fault zone following a hydrothermal reaction is closely related to porosity.

3.4. Changes in Geotechnical Properties of Basalts Taken from Different Points of the Same Formation

3.4.1. General Geological Assessment of the Sample Points

In this study, the serpentinization of olivines was found to be the most important factor affecting the strength and apparent porosity of basalts. Since serpentinization causes the internal expansion of the rocks, it is thought that micro-cracks developed especially in the M2 and M3 basalts due to the pressure. When the geological map of the study area is examined in Figure 1b, there is a volcano cone and two faults in the vicinity of the study area. There are also faults of different sizes (~4–20 km) in the south and south-west directions of the M3 basalts. Group M2 basalts are close to the fault contact, but farther from the volcano cone than group M3. A1 group basalts are located further away from both the volcano cone and faults. In addition, stratigraphically, the basalt field where the M3 samples were taken is at the top, the basalt field where the M2 samples were taken is on the lower level, and the basalt field where the A1 samples were taken is on the bottom level. It is concluded that the sample points at stratigraphically different elevations were affected by superficial alterations at different rates. In addition to the radial cracks formed during the placement of the volcano cone, the fractures caused by the fault lines may contribute to the deeper penetration of meteoric water, especially the reaction of olivine with water, and thus, serpentinization. The effect of the volcano cone and fault lines thus contributes indirectly to serpentinization.

3.4.2. Mineralogical and Petrographic Assessment of Basalts

Schaefer et al. [45] reported that geomechanical properties are difficult to measure due to the diversity of the materials that make up volcanic rocks and unknown micro-internal structures without detailed analyses of volcanic rocks. In this study, detailed petrographic analyses were performed and the serpentinization rates of olivines were investigated in detail for all rocks (Figure 8). In the figure, completely serpentinized anhedral olivine microcrystals and partially serpentinized subhedral olivine fenocrystals filling between plagioclase microliths are observed in the microlithic porphyritic-textured basalt sample. It is known that serpentine, which is a secondary mineral, has a much lower resistance compared to primary olivine. The serpentinization of olivine crystals increases the water absorption potential of the rocks and, therefore, the strength decreases. The serpentinization of olivine between plagioclase microlites causes the emergence of a kind of weak zone. This weak zone contributes to the easier failure of the rock under uniaxial pressure.

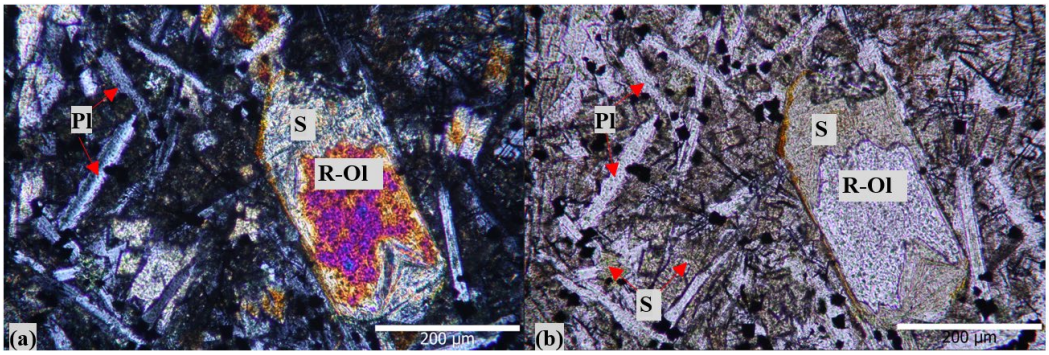

Figure 8. Partially serpentinizing olivine phenocrystals and wholly serpentinizing micro-granular olivines (cross-polarized light (**a**) and plane-polarized light (**b**)), Pl: plagioclase, S: serpentine, R-Ol: relict olivine.

3.4.3. SEM-EDS Analysis of Basalts

SEM images of basalt samples for A1, M2, and M3 are given in Figure 9a–c. The images demonstrate that each sample has different properties in terms of micro-cracks, texture, and pores. The SEM analyses indicated that M2 and M3 basalts have some microstructural defects like micro-cracks compared to A1. The SEM analysis also verified the results of geomechanical parameters for A1 basalts having intact rock properties. It was confirmed that the UCS was lower in the samples with a larger spread and width of micro-cracks.

In the current study, the effects of the alteration zones on the main chemical elements and microlithic textures were analyzed by EDS. According to the analysis of EDS, the main chemical elements of the basalts are O, Si, Al, Mg, Na, Fe, and Ca, indicating the main components of plagioclase, olivine, and augite, which can be seen in Figure 10a–d. Huang et al. [50] reported that serpentinization may reflect the influence of pyroxene minerals, which could release SiO_2 during peridotite serpentinization. Lamadrid et al. [51] stated that serpentinization also affects the physical and chemical properties of the oceanic lithosphere and the rate of the serpentinization of olivine slows down as the salinity increases and H_2O activity decreases. With serpentinization, the rock density decreases and the volume increases when 10–12% water is added. Thus, the rock becomes weaker [52,53]. Breuninger et al. [54] investigated the relationship of serpentinization with depth, joints, and faults observed in the dunites in a landslide area. In addition to the studies on the serpentinization of ultramafic rocks (dunite, harzburgite, etc.) in the literature, this study revealed how olivine serpentinization affected basalts geomechanically and mineralogically.

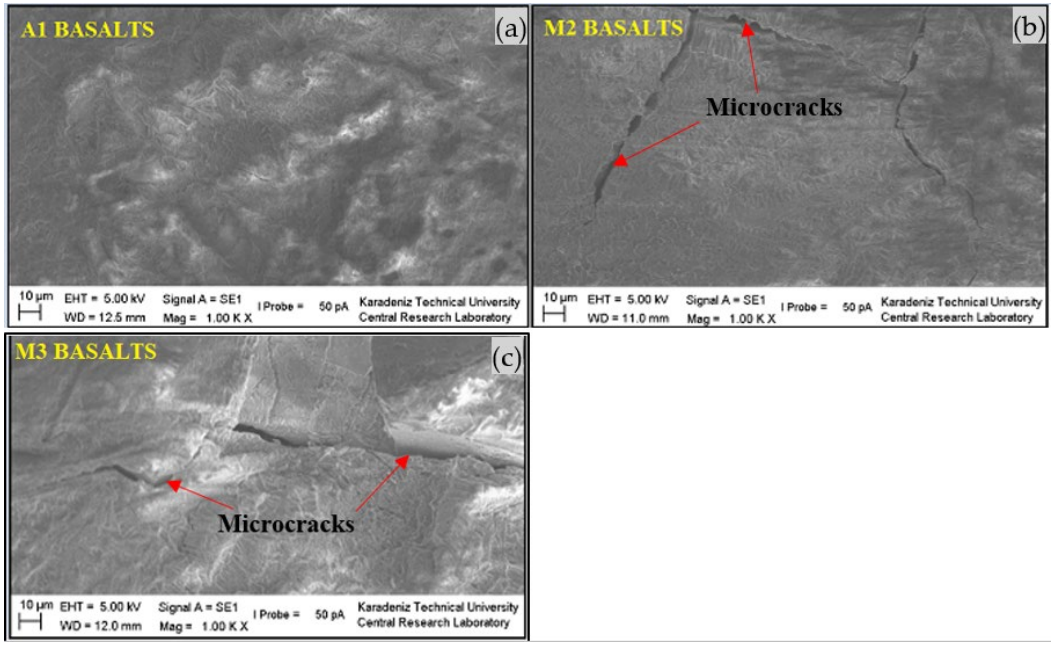

Figure 9. SEM images of the basalt samples; A1 (**a**), M2 (**b**), and M3 (**c**).

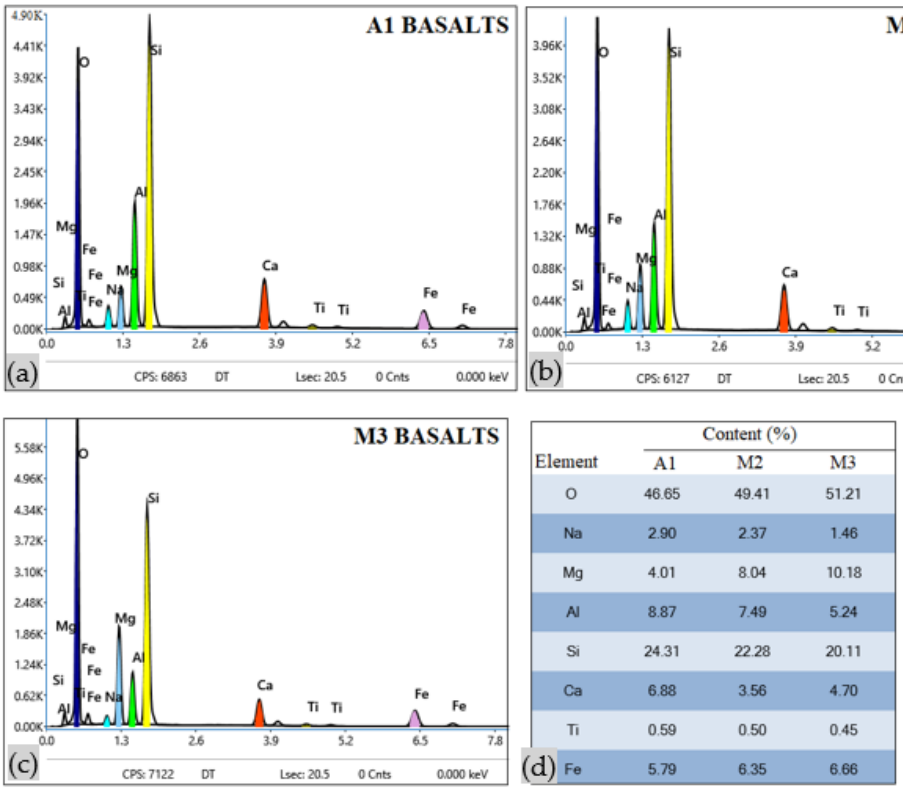

(d)

Element	Content (%)		
	A1	M2	M3
O	46.65	49.41	51.21
Na	2.90	2.37	1.46
Mg	4.01	8.04	10.18
Al	8.87	7.49	5.24
Si	24.31	22.28	20.11
Ca	6.88	3.56	4.70
Ti	0.59	0.50	0.45
Fe	5.79	6.35	6.66

Figure 10. Energy dispersion spectrum (EDS) diagrams of basalts (**a**–**c**) and chemical contents (**d**).

When samples are collected from a rock belonging to the same geological formation, it is often possible to obtain different experimental results depending on the alteration characteristics. Therefore, the use of the equations proposed in the literature for fresh samples in rocks with different alteration characteristics may lead to erroneous results. The importance of this study is to propose equations for the practical estimation of the UCS value in basalt rocks with different alteration characteristics. In cases where detailed analyses (petrographic, SEM-EDS, etc.) cannot be performed, whether basalts show alterations

or not can be estimated by examining the porosity values. Since a small change in porosity will cause significant changes in the rock strength, the change in the porosity values should be taken into account. While solid components are mainly considered in the geological nomenclature of rocks, from the engineer's point of view, pores, defects, and anisotropy are of a greater mechanical importance [3,55]. Basalts showing alterations between 8.25–75.5% were used in this study. The proposed equations for estimating the UCS are particularly significant for geotechnical applications where direct sampling is challenging, such as in weak rock environments. Further validation on a wider range of basaltic formations and alteration conditions will increase the robustness and applicability of the proposed equations. Therefore, further research is needed to compare the equations proposed in this study with a wider range of basaltic formations and alteration conditions.

4. Conclusions

Different geomechanical properties of basalts taken from different points of the same geological formation were demonstrated by experimental studies in the laboratory. Therefore, the reasons for these differences were investigated in detail from a general geological evaluation by field observations, petrographic thin section, and SEM-EDS analyses. According to the regression analyses, the UCS of basalts were found to be reliably estimated from the geomechanical properties (PLI, BTS, R, HL, UPV, etc.). Therefore, the proposed equations can be very crucial for weak rock environments where standard sampling is difficult, in cases of sample scarcity, and during the design phase of projects. In the current study, strong relationships were also obtained between the SR and geomechanical parameters of basalts. According to the thin-section analysis, the serpentinization of olivine, which is responsible for the differences in geomechanical properties, was obtained at 8.25% for A1, while this value was 24% for M2 and 75.5% for M3 basalts. In the geotechnical studies, sampling points are as important as the representative sample collection. Despite having the same lithology and age of formation, it should be kept in mind that quite different results can be obtained due to reasons such as proximity to the fault zone. In conclusion, since the variation in the porosity values may indicate the presence of alterations of the olivine in basalts, the equations proposed for these rocks in this study can be used with caution. Low levels of serpentine in basalts used in engineering works, such as concrete aggregates, are crucial for the long-term sustainability of structures.

Author Contributions: K.K.: methodology, experimental studies, writing—original draft preparation, statistical analysis, interpretation of results. H.K.: performing field investigations and collecting samples, petrographic examinations, and analysis of results. All authors have read and agreed to the published version of the manuscript.

Funding: This research received no external funding.

Institutional Review Board Statement: Not applicable.

Informed Consent Statement: Not applicable.

Data Availability Statement: The datasets generated during and/or analyzed during the current study are available from the corresponding author upon reasonable request.

Acknowledgments: The authors would like to express their gratitude to Lecturer Erdoğan Timurkaynak, Assist. M. Oğuz Sünnetci, and Lecturer Ümit Özsandık for their help during the laboratory studies, and to Yaşar Çakır for his contributions to the fieldwork.

Conflicts of Interest: The authors declare that they have no conflicts of interest.

References

1. Karaman, K.; Erçıkdı, B.; Kesimal, A. The assessment of slope stability and rock excavatability in a limestone quarry. *Earth Sci. Res. J.* **2013**, *17*, 169–181.
2. Zhang, X.; Altalbawy, F.M.A.; Gasmalla, T.A.S.; Al-Khafaji, A.H.D.; Iraji, A.; Syah, R.B.Y.; Nehdi, M.L. Performance of Statistical and Intelligent Methods in Estimating Rock Compressive Strength. *Sustainability* **2023**, *15*, 5642.

3. Karaman, K.; Bakhytzhan, A. Prediction of concrete strength from rock properties at the preliminary design stage. *Geomech. Eng*. **2020**, *23*, 115–125.
4. Wang, M.; Xu, W.; Chen, D.; Li, J.; Mu, H.; Mi, J.; Wu, Y. Summary of the Transformational Relationship between Point Load Strength Index and Uniaxial Compressive Strength of Rocks. *Sustainability* **2022**, *14*, 12456.
5. Jan, M.S.; Hussain, S.; e Zahra, R.; Emad, M.Z.; Khan, N.M.; Rehman, Z.U.; Cao, K.; Alarifi, S.S.; Raza, S.; Sherin, S.; et al. Appraisal of Different Artificial Intelligence Techniques for the Prediction of Marble Strength. *Sustainability* **2023**, *15*, 8835.
6. Ulusay, R.; Hudson, J.A. The complete ISRM suggested methods for rock characterization, testing and monitoring. In *Suggested Methods Prepared by the Commission on Testing Methods*; International society for rock mechanics ISRM: Ankara, Turkey; p. 628.
7. Kahraman, S. Evaluation of simple methods for assessing the uniaxial compressive strength of rock. *Int. J. Rock Mech. Min. Sci*. **2001**, *38*, 981–994.
8. Karaman, K.; Cihangir, F.; Erçıkdı, B.; Kesimal, A.; Demırel, S. Utilization of the Brazilian test for estimating the uniaxial compressive strength and shear strength parameters. *J. South. Afr. Inst. Min. Metall*. **2015**, *115*, 185–192.
9. Karaman, K. Evaluation of different surface characteristics and mineral grain size in the estimation of rock strength using the Schmidt Hammer. *Afr. Inst. Min. Metall*. **2024**, *124*, 173–184.
10. Tugrul, A.; Zarif, I.H. Correlation of mineralogical and textural characteristics with engineering properties of selected granitic rocks from Turkey. *Eng. Geol*. **1999**, *51*, 303–317.
11. Karaman, K.; Kesimal, A. Evaluation of the influence of porosity on the engineering properties of volcanic rocks from the Eastern Black Sea Region: NE Turkey, *Arab. J. Geosci*. **2015**, *8*, 557–564.
12. Kolay, E.; Baser, T. The effect of the textural characteristics on the engineering properties of the basalts from Yozgat region Turkey. *J. Geol. Soc. India*. **2017**, *90*, 102–110.
13. Tandon, R.S.; Gupta, V. The control of mineral constituents and textural characteristics on the petrophysical and mechanical (PM) properties of different rocks of the Himalaya. *Eng. Geol*. **2013**, *153*, 125–143.
14. Shakoor, A.; Bonelli, R.E. Relationship between petrographic characteristics, engineering index properties, and mechanical properties of selected sandstones. *Bull. Int. Assoc. Eng. Geol*. **1991**, *28*, 55–71.
15. Brace, W.F.. Dependence of fracture strength of rocks on grain size. In Proceedings of the 4th U.S. Symposium on Rock Mechanics (USRMS), University Park, PA, USA, March 1961; pp. 99–103.
16. Sonmez, H.; Gokceoglu, C.; Medley, E.W.; Tuncay, E.; Nefeslioglu, H.A. Estimating the uniaxial compressive strength of a volcanic bimrock. *Int. J. Rock Mech. Min. Sci.* **2006**, *43*, 554–561.
17. Ulusay, R.; Tureli, K.; VeIder, M.H. Prediction of engineering properties of a selected litharenite sandstone from its petrographic characteristics using correlation and multivariate statistical techniques. *Eng. Geol*. **1994**, *38*, 135–157.
18. Goodman, R.E. *Rock in Engineering Construction*; Wiley: New York, NY, USA, 1993; p. 412.
19. Saar, M.O.; Manga, M. Permeability-porosity relationship in vesicular basalts. *Geophys. Res. Lett*. **1999**, *26*, 111–114.
20. Gurocak, Z.; Kilic, R. Effect of weathering on the geo mechanical properties of the miocene basalts in Malatya, Eastern Turkey. *Bull. Eng. Geol. Environ*. **2005**, *64*, 373–381.
21. Juneja, A.; Endait, M. Laboratory measurement of elastic waves in basalt rock. *Measure* **2017**, *103*, 217–226.
22. Murthy, S.K.; Gupta, S.; Kumar, D.; Dixit, M. The effect of porosity on engineering properties of vesicular amygdaloidal basalts. *Int. J. Eng. Technol. Appl. Sci*. **2021**, *5*, 134–137.
23. Pathiranagei, S.V.; Gratchev, I.; Kong, R. Engineering properties of four different rocks after heat treatment. *Geomech. Geophys. Geol.* **2021**, *7*, 16.
24. Tahir, O.M.O.; Karaman, K. Prediction of the uniaxial compressive strength of basalts from the point load strength index using the conversion factor. *Gümüşhane Üniver. Fen Bilim. Enstitüsü Derg*. **2021**, *11*, 1242–1249. (In Turkish)
25. Liu, Z.; Zhang, C.; Wang, H.; Zhou, H.; Zhou, B. Effects of amygdale heterogeneity and sample size on the mechanical properties of basalt. *J. Rock Mech. Geotech. Eng*. **2022**, *14*, 93–107.
26. Tarawneh, K.; Amaireh, M.; Abdelhadi, N.; Titi, A.; Dweirj, M. Characterization of the physical and mechanical properties of the harrat ash shaam basalt (HASB)/Northeast Jordan. *Open J. Civil Eng*. **2022**, *12*, 463–475.
27. Ye, Z.; Liu, X.; Sun, H.; Dong, Q.; Du, W.; Long, Q. Variations in permeability and mechanical properties of basaltic rocks ınduced by carbon mineralization. *Sustainability* **2022**, *14*, 15195.
28. Sharo, A.A.; Al-Tawaha, M.S. Prediction of engineering properties of basaltic rocks in Jordan. *Int. J. Civ. Eng Technol.* **2019**, *10*, 1731–1739.
29. Yucel, C.; Arslan, M.; Temizel, İ.; Abdioglu, E. Volcanic facies and mineral chemistry of Tertiary volcanics in the northern part of the Eastern Pontides, northeast Turkey: Implications for pre-eruptive crystallization conditions and magma chamber processes. *Mineral. Petrol.* **2014**, *108*, 439–467.
30. Leeb, D. New dynamic method for hardness testing of metallic materials *Rev. Metal.* **1979**, *15*, 57–63.
31. Desarnaud, J.; Kiriyama, K.; Simsir, B.; Wilhelm, K.; Viles, H. A laboratory study of equotip surface hardness measurements on a range of sandstones. What influences the values and what do they mean. *Earth Surf. Process. Landf*. **2019**, *44*, 1419–1429.
32. Korkanc, M.; Tugrul, A.M. Evaluation of selected basalts from Niğde. Turkey. as source of concrete aggregate. *Eng. Geol*. **2004**, *75*, 291–307.
33. Toft, P.B.; Arkani-Hamed, J.; Haggerty, S.E. The effects of serpentinization on density and magnetic susceptibility. a petrophysical model. *Phys. Earth Planet. Inter*.**1990**, *65*, 137-157.

34. Kahraman, S.; Gunaydin, O.; Fener, M. The effect of porosity on the relation between uniaxial compressive strength and point load ındex. *Int. J. Rock Mech. Min. Sci*.**2005**, *42*, 584–589.
35. Kılıc, A.; Teymen, A. Determination of mechanical properties of rocks using simple methods. *Bull. Eng. Geol. Environ*. **2008**, *67*, 237–244.
36. Diamantis, K.; Exarhakos, G.; Migiros, G.; Gartzos, E. Evaluating the triaxial characteristics of ultamafic rocks from central Greece using the physical, dynamic and mechanical properties. *Open Access Libr. J.* **2016**, *3*, 1–20.
37. Schuiling, R.D. Troodos: A giant serpentinite diapir. *Int. J. Geosci.* **2011**, *2*, 98–101.
38. Moody, J.B. Serpentinization: A review. *Lithos* **1976**, *9*, 125–138.
39. Kelemen, P.B.; Hirth, G. Reaction-driven cracking during retrograde metamorphism: Olivine hydration and carbonation. *Earth Planet Sci. Lett.* **2012**, *345*, 81–89.
40. Allen, D.E.; Seyfried, W.E. Compositional controls on vent fluids from ultramafic-hosted hydrothermal systems ad mid-ocean ridges: An experimental study at 400 °C, 500 bars Geochim. Cosmochim. *Acta* **2004**, *67*, 1531–1542.
41. Streit, E.; Kelemen, P.; Eiler, J. Coexisting serpentine and quartz from carbonate-bearing serpentinized peridotite in the Samail Ophiolite, Oman. *Contrib Miner. Petrol*. **2012**, *164*, 821–837.
42. O'Hanley, D.S. Solution to the volume problem in serpentinization. *Geology* **1992**, *20*, 705–708.
43. Jamtveit, B.; Putnis, C.V.; Malthe-Sørenssen, A. Reaction induced fracturing during replacement processes. *Cont. Miner. Petrol.* **2009**, *157*, 127–133.
44. Farough, A.; Moore, D.E.; Lockner, D.A.; Lowell, R.P. Evolution of fracture permeability of ultramafic rocks undergoing serpentinization at hydrothermal conditions : An experimental study. *Geochem. Geophys. Geosystems* **2015**, *16*, 44–55.
45. Schaefer, L.N.; Kendrick, J.E.; Oommen, T.; Lavallée, Y.; Chigna, G. Geomechanical rock properties of a basaltic volcano. *Volcanology* **2015**, *3*, 29.
46. Pappalardo, G.; Punturo, R.; Mineo, S.; Contrafatto, L. The role of porosity on the engineering geological properties of lavas from Mount Etna. *Eng. Geol*. **2017**, *221*, 16–28.
47. Heap, M.J.; Xu, T.; Chen, C. The influence of porosity and vesicle size on the brittle strength of volcanic rocks and magma. *Bull. Volcanol*. **2014**, *76*, 856.
48. Hatakeyama, K.; Katayama, I. Pore fluid effects on elastic wave velocities of serpentinite and implications for estimates of serpentinization in oceanic lithosphere. *Tectonophysics* **2020**, *775*, 228309.
49. Tenthorey, E.; Cox, S.F.; Todd, H.F. Evolution of strength recovery and permeability during fluid-rock reaction in experimental fault zones. *Earth Planet. Sci. Lett*. **2003**, *206*, 161–172.
50. Huang, R.; Sun, W.; Song, M.; Ding, X. Influence of pH on Molecular Hydrogen (H_2) Generation and Reaction Rates during Serpentinization of Peridotite and Olivine. *Minerals* **2019**, *9*, 661.
51. Lamadrid, H.M.; Rimstidt, J.D.; Schwarzenbach, E.M.; Klein, F.; Ulrich, S.; Dolocan, A.; Bodnar, R.J. Effect of water activity on rates of serpentinization of olivine. *Nat. Commun.* **2017**, *8*, 16107.
52. Escartin, J.; Hirth, G.; Evans, B. Strength of slightly serpentinized peridotites: Implications for the tectonics of oceanic lithosphere. *Geology* **2001**, *29*, 1023–1026.
53. Deschamps, F.; Godard, M.; Guillot, S.; Hattori, K. Geochemistry of subduction zone serpentinites: A review. *Lithos* **2013**, *178*, 96–127.
54. Breuninger, T.; Menschik, B.; Demharter, A.; Gamperl, M.; Thuro, K. Investigation of critical geotechnical, petrological and mineralogical parameters for landslides in deeply weathered dunite rock (Medellín, Colombia). *Int. J. Environ. Res. Public Health* **2021**, *18*, 11141.
55. Franklin, J.A. Classification of Rock According to Its Mechanical Properties. Ph.D. Dissertation, University of London Imperial College, London, UK 1970.

Disclaimer/Publisher's Note: The statements, opinions and data contained in all publications are solely those of the individual author(s) and contributor(s) and not of MDPI and/or the editor(s). MDPI and/or the editor(s) disclaim responsibility for any injury to people or property resulting from any ideas, methods, instructions or products referred to in the content.